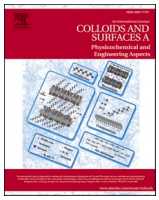
Colloids and Surfaces A: Physicochemical and Engineering Aspects 687 (2024) 133444



Contents lists available at ScienceDirect

Colloids and Surfaces A: Physicochemical and Engineering Aspects

journal homepage: www.elsevier.com/locate/colsurfa





The DFT and in-silico analysis of 2,2′-((1e,1′e)-((3,3′-dimethyl-[1,1′-biphenyl]−4,4′ diyl)bis(azanylylidene)) bis(methanylylidene))diphenol molecule

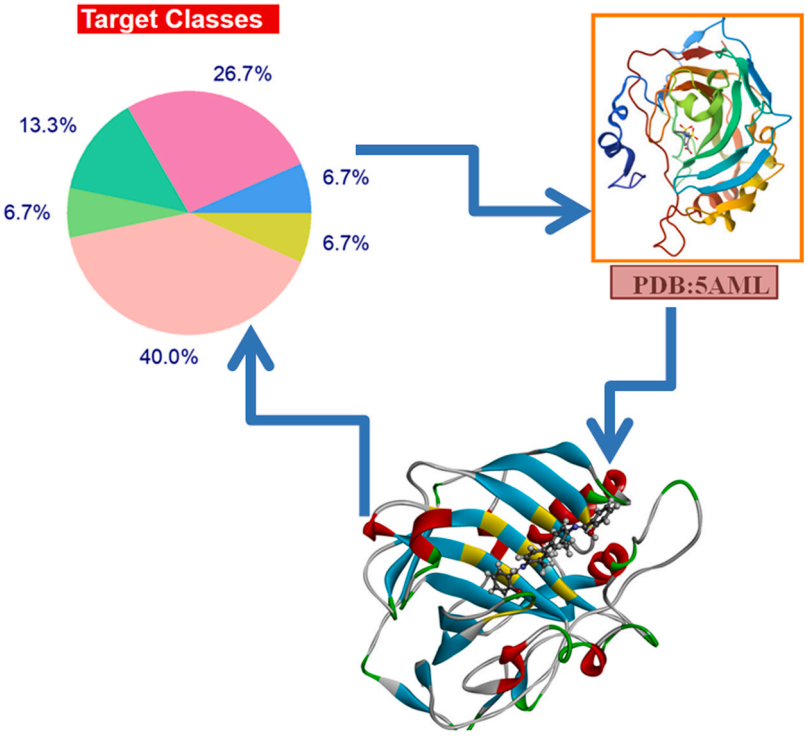
Yusuf Sert [a,*], Mustafa R. Albayati [b], Fatih Şen [a], Necmi Dege [c]

[a] Sorgun Vocational School, Bozok University, Yozgat 66100, Turkey
[b] College of Education, Department of Chemistry, Kirkuk University, Kirkuk, Iraq
[c] Department of Physics, Faculty of Arts and Sciences, Ondokuz Mayıs University, Samsun, Turkey

HIGHLIGHTS

- Frequency analysis, optimized structures and electronic energy values of the title molecule were investigated.
- The theoretical vibrational frequencies were analyzed with PED analysis.
- Molecular docking study was conducted with Autodock Vina.
- Drug-Likeness Properties and ADME analysis was researched.

GRAPHICAL ABSTRACT



* Corresponding author.
E-mail address: yusuf.sert@bozok.edu.tr (Y. Sert).

https://doi.org/10.1016/j.colsurfa.2024.133444
Received 26 December 2023; Received in revised form 25 January 2024; Accepted 7 February 2024
Available online 11 February 2024
0927-7757/© 2024 Elsevier B.V. All rights reserved.

ARTICLE INFO

Keywords:
Vibrational spectroscopy
Density Functional Theory
Molecular docking, ADME

ABSTRACT

In this study, crystallographic, molecular geometry, surfaces (MEP, Hirshfeld and Frontiers Orbitals-HOMO and LUMO), molecular docking with carbonic anhydrase II-5AML protein, drug-likeness, ADME and vibrational assignment analyses of the molecule were studied in detail and the results were carefully analyzed. The theoretical studies were carried out in DFT/B3LYP/6–311++G(d,p) quantum chemical method and basis set with the Gaussian 09 W package program. Potential energy distributions (PED) were used in conjunction with the VEDA 4 tool to get the vibrational assignments of the title chemical with %10 precision. In solid phase, the FT-IR experimental spectrum was collected at 4000–400 cm^{-1}. Due to the affinity and binding energy of the title molecule to protein active sites, the results showed that our molecule is a potent potential inhibitor of carbonic anhydrase II.

1. Introduction

Schiff bases are the compounds carrying imine or azomethine (–C═N–) functional group [1,2]. These are the condensation products of primary amines with carbonyl compounds and were first reported by Hugo Schiff [1]. Schiff bases belong to a widely used group of organic intermediates important for production of specialty chemicals, e.g. pharmaceuticals, or rubber additives and as amino protective groups in organic synthesis [3]. They have a wide range of biological functions, including antimalarial, antiprotozoal, antitumor, antifungal, antibacterial, analgesic, anti-inflammatory, antioxidant, cardiovascular, antitubercular, and used as local painkillers, as well as they have extensive applications in organometallic chemistry, catalysis, removal dyes [4]. Among the various hetero-atom containing compounds, Schiff bases are quite effective because of the presence of a nitrogen atom, and several such compounds have been reported in the literature as potential corrosion inhibitors for metals and alloys in an acidic medium [5,6]. The growing popularity of Schiff bases as corrosion inhibitors is primarily based on their low toxicity and convenience of synthesis from very inexpensive starting materials [5,6]. Bis-Schiff bases have gained an importance as anti-tumor agent [7]. Recently, 4,5,6,7-tetrahydrobenzo [*d*]thiazole-based Schiff-bases were screened for their in vitro anti-cancer activity against the cell lines MCF-7 and HepG2 [8]. Bis-Schiff bases of pyrazoles, were investigated for their in vitro anti-proliferation activity toward three human carcinoma cell lines, and the results indicated that these compounds were promising [9]. A series of bis-pyrimidine Schiff bases were synthesized and screened for its anticancer potentials. The molecular docking study was carried to find the interaction between active molecules with receptor. The results showed that some of these Bis-Schiff's bases are potent anticancer molecules [10]. Based on the above considerations and further to our efforts in synthesis and study new bio-active Schiff bases [11–13] we reported herein the synthesis of new bis-Schiff base namely 2,2′-((1e, 1′e)-((3,3′-dimethyl-[1,1′-biphenyl]−4,4′ diyl)bis(azanylylidene))bis (methanylylidene))diphenol.

It is evident from the theoretical and experimental research on molecules done thus far that the title compound has not been studied. For the first time, molecular docking studies with SwissTarget analyses (to predict its binding affinities and specificities by docking simulation, to understand its important intermolecular interactions with two different protein targets) and highest occupied molecular orbital (HOMO)–lowest unoccupied molecular orbital (LUMO), Hirshfeld, and molecular electrostatic potential analysis were carried out. Finally, the drug similarity and drug potential of the molecule we are working on has also been investigated for the first time.

2. Experimental and computational method details

Using a PerkinElmer Spectrum Two FT-IR spectrometer, the Fourier transform infrared (FT-IR) spectrum (400–4000 cm^{-1}) was acquired in the solid phase at ambient temperature at intervals of 4 cm^{-1}. Without any restrictions for the computational process, the molecular geometry was extracted from the X-ray diffraction experimental output (*cif file output). Gaussian 09 W software was utilized [14]. The density functional theory (DFT) approach was used to do theoretical calculations of the chemical under investigation [15,16]. One of the most popular exchange-correlation functions, B3LYP, which combines Lee, Yang, and Parr's correlation function [17] and Becke's three-parameter exchange function [18], was employed in the DFT computations. Using the improved structure, the harmonic vibrational frequencies were calculated at the same theoretical level. Both the molecular visualization application GaussView5 [19] and the program VEDA 4 [20,21] were used to assign vibrational bands. Using Crystal Explorer 3.1 [22], the Hirshfeld surface analysis was carried out over the cif* file. The drug likeness and ADME analysis were carried out online with SwissADME [23], after the molecular docking studies involving the title molecule were completed using the software Auto Dock Vina [24].

2.1. Synthesis part

A mixture of (2 mmol) salicaldehyde with (1 mmol) of 3,3′-dimethylbiphenyl-4,4′-diamine in 25 ml of ethanol was refluxed for 7 hr. The mixture was cooled and the precipitate was collected, dried and recrystallized from Dioxan to afford the title compound as an orange crystals with m.p. = 209–211 ℃. All chemical reagents used were purchased from Fluka, Sigma-Aldrich chemicals and were then used without any purification.

2.2. Crystallographic analysis

A fitting optically clear single crystal sample of size 0.72 × 0.32 × 0.06 mm was chosen by means of MITUTOYO 377–972 A Stereo Microscope for the analysis of single-crystal X-ray diffraction. Data collection was performed on a STOE IPDS 2 (STOE & Cie GmbH Hilpertstrasse 10 64295 Darmstadt | Germany) diffraction measurement device by the rotation method using monochromatic Mo K-α radiation (λ = 0.71073 Å) at 293 K.

The crystal structure was solved by direct methods using SHELXS-97 [25] and molecular skeleton of compound was revealed. All non-hydrogen atoms were refined with anisotropic parameters by ANIS command. H atoms were placed geometrically at distances of 0.93 Å (CH), 0.96 Å (CH_3) from the parent C atoms and at distance of 0.820 Å (OH) from the parent O atoms. The molecular geometry was refined by full-matrix least-squares methods on F^2 utilizing SHELXL-2018/1 [26]. Details of crystal data, data collection and refinement are given in Table 1. The following programs were used in analysis: ORTEP-III [27] for the molecular visualization and PARST [28,29] for the identification of hydrogen bondings in the WinGX crystallographic software package [27] were used in crystal structure determination.

3. Molecular geometry

The title compound, 2,2′-((1*E*,1′*E*)-((3,3′-dimethyl-[1,1′-biphenyl]−4,4′-diyl)bis(azanylylidene))bis(methanylylidene))diphenol,

Table 1
Crystallographic data for the compound.

Chemical formula	$C_{28}H_{24}N_2O_2$
Formula weight	420.49
F(000)	888
Radiation, graphite monochr.	MoK_α (λ = 0.71073 Å)
Crystal system	Orthorhombic
Space group	*Pna2₁*
a, *b*, *c* (Å)	34.284 (4), 4.6907 (4), 13.3935 (15)
α, β, γ (°)	90
Volume (Å^3), Z	2153.9 (4), 4
Crystal dimension (mm)	0.72 × 0.32 × 0.06
Temperature (*K*)	293
D_{calc} (mg m^{-3})	1.297
Measured reflections	9408
Independent reflections	3627
No of reflections with I>2 $\sigma(I)$	1636
θ range (°)	1.2–24.6
Range of h, k, l	-40<h<39, −4<k<5, −15<l<15
Refinement on	F^2
Calculated weights	$w = 1/[\sigma^2(F_o^2) + (0.0991\ P)^2]$ where $P = (F_o^2 + 2\ F_c^2)/3$
Number of refinement parameters	292
S	0.87
R [$F^2 > 2\sigma(F^2)$)]	0.075
wR (F^2)	0.195
$(\Delta\rho)_{max}$ (e Å^{-3}), $(\Delta\rho)_{min}$ (e Å^{-3})	0.34, −0.20

$C_{28}H_{24}N_2O_2$, an ORTEP-3 [27] view with the atomic numbering is shown in Fig. 1**a.**

The single crystal X-ray diffraction studies indicated that the compound crystallizes in the orthorhombic lattice in space group *Pna2₁* (Hall symbol P 2c −2n and H-M symbol n a 21). It has the unit cell dimensions: a = 34.284 (4) Å, b =4.6907 (4) Å, c = 13.3935 (15) Å, α=β=γ=90° and number of formula units in the unit cell Z = 4.

The molecular structure is contained two Schiff base, two hydroxyl and two methyl groups in addition to the four benzene rings. The Schiff base (N═C) bonds are 1.249 (11) Å for N1=C7 and 1.268 (12) Å for N2=C22, which agrees with lengths published in literature 1.277 (3) Å [30], 1.288 (4) Å [31], 1.278 (3) and 1.275 (3) Å [32], etc. The C—CH_3 bond length of 1.512 (13) Å of C13—C14 and the C—OH bond length of 1.369 (12) of C1—O1 Å are too close to the C-CH_3 bond length of 1.526 (13) Å in C20—C21 and the C-OH bond length of 1.391 (12) Å in C28—O2, respectively. Despite close to seeming planar of molecular structure of compound, the dihedral angles between the plane A (C1/2/3/4/5/6), the plane B (C8/9/10/11/12/13), the plane C (C15/16/17/18/19/20) and the plane D (C23/24/25/26/27/28) are 5.34° (A/B), 15.68° (A/C), 10.21° (A/D), 10.39° (B/C), 5.92° (B/D) and 7.01° (C/D).

The analysis results by means of the PARST [28,29] showed that there are considerable six intramolecular and two intermolecular interactions, details of which are provided in Table 2**.** Intramolecular interactions have formed S- type hydrogen bonding motifs (Fig. 2). The bondings and motifs are as follows:

- S(6) motifs: O1—H1•••N1 and O2—H2•••N2
- S(5) motifs: C14—H14*A*•••N1 and C21—H21*A*•••N2
- S(4) motifs: **1-** O1—H1•••N1, C14—H14*A*•••N1, C14—H14*A*•••O1 and **2-** O2—H2•••N2, C21—H21*A*•••N2, C21—H21*A*•••O2.

In here;

- N1 and N2: bifurcated acceptor atoms
- C14 and C21: bifurcated donor atoms (*via* H14A and H21A)
- O1 and O2 bifurcated donor/acceptor atoms

plays a role in S(4) motif formations. The crystal structure is stabilized by two C–H•••$O_{hydroxyl}$, in which the atom O2 in the molecule at (−x+1, −y+2, z+1/2) acts as hydrogen-acceptor, via atom H17, to atom C17 in the molecule at (x, y, z) and atom O1 in the molecule at (−x+1/2, y+1/2, z−1/2) acts as hydrogen-acceptor, via atom H9, to atom C9 in the molecule at (x, y, z). There are no any C—H•••π and π−π stacking (face-to-face) interactions in the crystal structure.

The quantum mechanical computational modeling calculations were carried out using B3LYP/6–311++G(d, p) level of Density Functional Theory (DFT) method. The *.gjf file obtained from the *.res file was used as the input geometry. The optimization was conducted with default spin, solvent-free on the ground state. The ball and bond type drawing for the calculated molecular structure are presented in Fig. 1**b**. The electronic structure parameters for the theoretical molecule were summarized as follows: E(RB3LYP): −1341.76485050 a.u.; dipole moment: 1.3076 debye; entropy: 186.541 cal/mol-K; heat capacity: 107.807 cal/mol-K.

The optimized geometry shows that the Schiff base bond lengths calculated as 1.28896 and 1.28909 Å are longer than from X-ray data. The molecule is not planar which can be seen from the torsion angles: 143.56615° (C7/N1/C8/C13), −142.39385°(C22/N2/C19/C20), −141.17659° (C10/C11/C16/C17) and −140.81961° (C15/C16/C11/C12). The calculated D—H, H—A, D—A lengths and D—H•••A angle for the intra-molecular bondings are listed in Table 2.

The DFT/B3LYP/6–311++G(d, p) geometry has been compared with the X-ray molecular structure by the correlation (R^2) and superimposition (root-mean-square-RMS) methods. According to the some selected structural parameters are listed in Table 3, the computed R^2 (R-squared) values are 0.8598 (y=0.8064x+0,2738) for bond lengths, 0.7734 (y=0,8572x+16,757) for bond angles, 0.9991 (y=0,8119x+33,324) for torsion angles at 6–311++G(d, p) level. The overlap of molecular skeletons using by the atom-by-atom superimposition method are given in Fig. 1**c**, which red and black colors have been represented the X-ray molecular structure and theoretical geometry, respectively. RMS results obtained after 21 iterations of the minimization process: 0.524 (RMS Error), 0.189 (RMS Gradient) and 0.0005 (RMS Move). Both R^2 and RMS values demonstrate DFT/B3LYP/6–311++G(d, p) geometry fits so well X-ray molecular structure.

4. Surface studies

4.1. MEP surface

To determine the reactive regions for electrophilic (electron-rich, most electro negative electrostatic potential) and nucleophilic attack (electron-poor, most positive electrostatic potential), the molecular electrostatic potential surface (MEPS) were calculated with Gaussian09W [14] and viewed with the Gauss-View 5.0 [19] software by using the gaussian checkpoint file (*.chk). The MEPS were mapped for molecule as shown in Fig. 3, where is in the energy (a.u) range of the map color, from −3.922 e-2–3.922 e-2, corresponds to red and blue colors, respectively.

The red regions represent electron-rich regions, while the blue regions represent electron-poor regions. Order of increasing electron density is blue < green < yellow < orange < red. **In** Fig. 3, the red regions are located above the atoms O1 and O2 in MEPS. These regions are in good agreement with the atoms O1 and O2, which play the role of acceptors in hydrogen bondings.

4.2. Hirshfeld surface

Hirshfeld surface analysis [33] was performed to investigate intermolecular interactions and to determine the contribution of these interactions to the packing of the crystal structure. Hirshfeld surface is mapped using the normalized contact distance (d_{norm}) which is defined in terms of external (d_e) and (d_i) internal distances, and the van der Waals (vdW) radii of atoms [33] and is visually represented utilizing a color scheme of red, white, and blue. In this scheme, shorter contacts are depicted in red, contacts around the van der Waals separation are

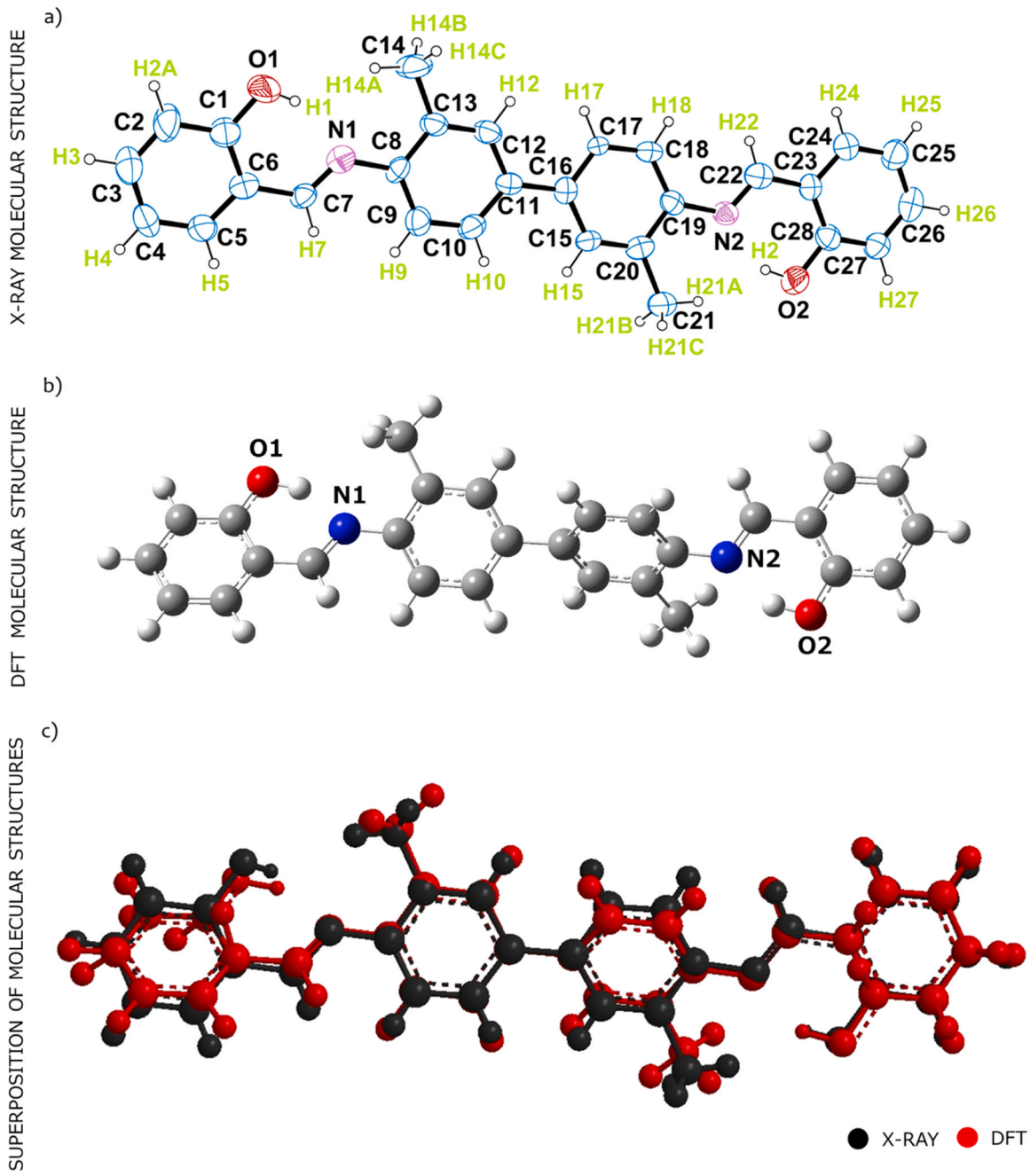


Fig. 1. a) A view of the title compound showing the atom-numbering scheme at the 50% probability level. **b)** Theoretical (DFT/B3LYP/6–311++g(d, p)) molecular structure. **c)** Atom-by-atom superimposition of the optimized structure DFT/B3LYP/6–311++g(d, p) (red) over the X-ray structure (black) for compound.

Table 2
Hydrogen-bond geometry (Å, º).

D—H•••A	D—H		H•••A		D•••A		D—H•••A	
	X-ray	DFT	X-ray	DFT	X-ray	DFT	X-ray	DFT
O2—H2•••N2	0.82	0.99	1.85	1.74	2.567 (7)	2.636	146	147.65
O1—H1•••N1	0.82	0.99	2.02	1.74	2.566 (8)	2.637	123	147.66
C21—H21*A*•••O2	0.96	1.09	2.69	3.43	3.640 (9)	4.093	173	119.41
C21—H21*A*•••N2	0.96	1.09	2.31	2.84	2.810 (9)	2.856	112	79.70
C14—H14*A*•••N1	0.96	1.09	2.32	2.83	2.807 (10)	2.857	111	80.43
C14—H14*A*•••O1	0.96	1.09	2.69	3.43	3.643 (9)	4.076	171	120.18
C17—H17•••O2^{i}	0.93	1.08	2.98		3.616 (8)		127	
C9—H9•••O1^{ii}	0.93	1.08	2.66		3.458 (9)		145	

Symmetry codes: (i) −x+1, −y+2, z+1/2; (ii) −x+1/2, y+1/2, z−1/2.

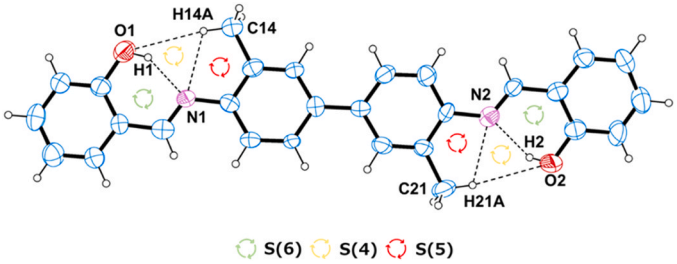


Fig. 2. Intramolecular hydrogen bonding motif formations.

Table 3
Some selected bond distances, bond angle, torsion angles.

Structural parameters Bond distances (Å)	X-ray Diffraction	DFT/B3LYP/6–311++G (d, p)
C1—O1	1.369 (12)	1.342
C1—C2	1.392 (15)	1.400
C5—C6	1.403 (14)	1.408
C6—C7	1.453 (13)	1.450
N1—C7	1.249 (11)	1.289
N1—C8	1.420 (11)	1.408
C8—C9	1.373 (12)	1.401
C12—C13	1.365 (13)	1.393
C10—C11	1.388 (13)	1.401
C11—C16	1.480 (10)	1.482
C16—C17	1.396 (12)	1.401
C19—C20	1.403 (12)	1.411
C19—N2	1.444 (11)	1.408
C20—C21	1.526 (13)	1.508
N2—C22	1.268 (12)	1.289
C22—C23	1.432 (13)	1.450
C28—O2	1.391 (12)	1.342
C25—C26	1.364 (15)	1.401
Bond angles (°)		
C2—C1—O1	120.2 (11)	118.7
C6—C1—O1	118.9 (9)	121.8
C6—C7—N1	123.7 (9)	122.6
C7—N1—C8	123.5 (8)	121.1
C13—C8—N1	117.2 (8)	118.5
C1—O1—H1	109.5	107.4
C9—C8—N1	124.1 (9)	121.9
C10—C11—C12	113.7 (8)	117.7
C11—C16—C17	121.6 (7)	121.2
C18—C19—N2	126.3 (8)	122.0
C28—O2—H2	109.5	107.4
C19—N2—C22	120.8 (9)	121.2
N2—C22—C23	120.2 (9)	122.6
C22—C23—C24	120.0 (10)	119.8
C22—C23—C28	124.1 (9)	121.4
C23—C28—O2	118.9 (9)	121.8
Torsion angles (°)		
O1—C1—C6—C5	179.0 (11)	179.7
C14—C13—C8—C9	178.8 (10)	178.4
C19—N2—C22—C23	179.2 (8)	176.4
C7—N1—C8—C9	5.0 (14)	40.3
N2—C22—C23—C24	179.2 (9)	179.5
O2—C28—C27—C26	179.2 (9)	179.7
C10—C11—C16—C15	9.8 (11)	38.3

represented in white, and longer contacts are displayed in blue [33–36].

The Hirshfeld surface mapped with d_{norm} for the title compound and fingerprint plots were generated with the Crystal Explorer 21.5 [37] software by using the crystallographic information file (CIF) obtained from crystal structure solution. Surface (Fig. 4) was monitorized with the following details: fixed color scale of −0.1175 (red) to 1.4181 Å (blue); 529.55 A^3 volume; 479,19 A^2 area; 0661 globularity; 0606 asphericity. For the compound, there are eight red spots in d_{norm} surface (Fig. 4**)**.

The 2-D representation of a Hirshfeld surface, known as the fingerprint plot, is depicted in Fig. 5**a** and Fig. 5**b** shows the percentages of all interactions observed. The H···H/H···H interaction type holds the highest percentage contribution at 56.1%, followed by C···H/H···C (17.3%), C···C/C···C (12.3%), and O···H/H···O (9.7%). In particular, contributions from H···H/H···H and C···H/H···C contacts are represented by sharp spikes plot, as shown in Fig. 5**a**.

4.3. Frontier orbital surface

The terms LUMO (Lowest Unoccupied Molecular Orbital) and HOMO (Highest Occupied Molecular Orbital), also known as FMOs (Frontier Molecular Orbitals), are crucial for the analysis and interpretation of a wide range of molecular properties, including global reactivity descriptors, charge transfers, polarizability, hardness, softness, excitability, basicity, and acidity [38–43]. Theoretically, the molecule under examination was computed LUMO and HOMO energy values of −6.235 eV, −8.822 eV, and a |HOMO-LOMO| energy band gap of 2.587 eV. According to Costa et al. [44], organic semiconductor materials need an energy band gap (|HOMO-LOMO|) of less than 3 eV. With an energy band gap of 2.587 eV, our compound in this study can be exploited as an organic semiconductor material in this regard. In addition, other theoretical global descriptors depending on the HOMO and LUMO energies are listed in Table 4. Accordingly, ionization potential 8.822, electron affinity 6.235, chemical hardness 1.293, chemical softness 0.387 eV, electronegativity 7.529 eV, chemical potential −7.529 eV, electrophilic index 21.912 eV and maximum charge transfer index 5.821 eV were calculated.

Finally, the HOMO and LUMO distributions of the molecule are given in Fig. 6. As can be seen from Fig. 6, HOMO distributions were distributed almost everywhere in the molecule, while LUMO distributions were similar except for the methyl groups at the top and bottom of the molecule.

5. Molecular docking study

Molecular docking has grown in importance recently for medication development. The atomic-level interaction between a small molecule and a protein may be described using this method, which also allows us to define the behavior of small molecules in target protein binding sites and clarify important biochemical processes. This topic has been the subject of several theoretical studies [45–47]. In this section, molecular docking between the title ligand and the human carbonic anhydrases II-PDB: 5AML-A chain was carried out using the AutoDock Vina tool [24]. The target (PDB: 5AML) that will be worked on in this instance was selected by looking at the percentage distributions in Fig. 7 and reading through the pertinent literature [48–50], using the online SwissTarget database [51]. The protein data bank provided the X-ray structure of carbonic anhydrase II (PDB: 5AML-A chain) [52] and polar hydrogens were added after the heteroatoms were removed. The optimized structure of the ligand was calculated by using DFT-B3LYP/6–311++G(d,p). Everything was prepared using the Discover Studio Visualizer 4.0 (DSV 4.0) [53] (both ligand and receptor). Here at first, the active residues of the PDB: 5AML-A chain were labeled as: THR200, THR199, LEU198, PHE131, VAL121, HIS119, HIS96, HIS94, GLN92, ASN67, ASN62 for hCAII /PDB: 5AML. The grid parameters were designed with the following active regions included: hCAII /PDB: 5AML; 32×40×32 $Å^3$ x, y,z dimensions; 0.375 Å space; and −5.915, 5.359, 16.391 x,y,z centers. Table 5 showed the interaction's rmsd l.b and rmsd u.b values, as well as the final molecular docking scores. Additionally, 3D (a), 2D (b) shapes of the docking and the position of the molecule within the protein were indicated in Fig. 8. The best docking score was obtained in first mode using the binding energies=−8.8 kcal/mol from Table 5. The inhibition constant of the docking was computed as 0.354448 μM using the Ki=exp (G/RT) equation (''G-binding energy, R-gas constant=1.9872036×10^{-3} kcal/mol, and T-temperature=298.15 K''). According to the Fig. 8(b), the conventional hydrogen bonding between THR199 residue and H3 atom (according to the numbering format of the optimized structure)

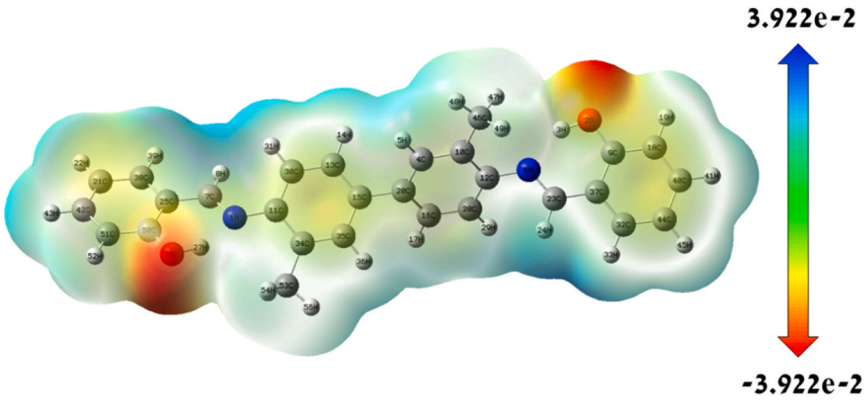


Fig. 3. The Molecular Electrostatic Potential Surface (MEPS) for the optimized geometry [DFT/B3LYP/6–311++G(d, p)].

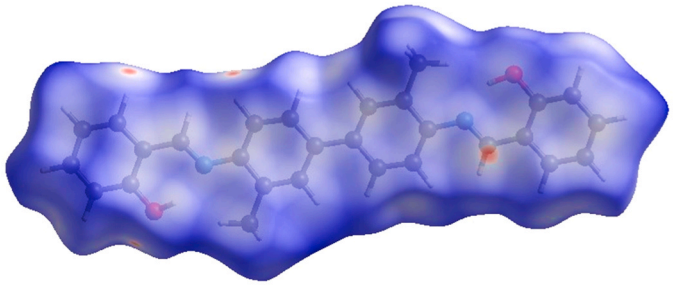


Fig. 4. The Hirshfeld surface of compound mapped with d_{norm}.

was found as 2.91 Å. Additionally, as seen from the Fig. 8, van der Waals, carbon-hydrogen, π-alkyl, π-cation, π donor hydrogen, π-σ and π-π-T shaped interactions and their bond lenghts were shown. When the molecular docking and inhibition constant results obtained are evaluated, we can say that the molecule we are working on is a good carbonic anhydrase II inhibitor.

6. Drug-likeness properties and ADME

It's common knowledge that the variety of physicochemical characteristics that commercially available medications contain characterizes "drug-likeness." The rule of five, or Ro5, was first introduced in 1997 and is sometimes referred to as a "drug-like" rule. However, its main goal was to address oral drugs' poor solubility and permeability, as it set limits on molecular weight (MW) of less than 500, lipophilicity (cLogP) of less than 5, the H-bond donor count (sum of OH+NH groups) of less than 5, and the H-bond acceptor count (sum of O+N atoms) of less than 10 [54,55]. For our compound, these quantities were obtained by using SwissADME web server [23] as follows: MW=420.50 g/mol, number of rotable bond=5, number of H-bond acceptor=4, number of H-bond donor=2, molar refractivity=133.25 $Å^2$, TPSA (topological polar surface area)=65.18 $Å^2$, MLOGP=4.29. Within the limits established according to these values, when the rules established by Lipinski were tested, it was seen that there was only one violation, which occurred in the MLOGP value. This is a very good result in terms of drug-likeness. In second step, the bioavailability radar (a) and boiled-egg shape (b) of the title compound was obtained as seen in Fig. 9 by using the same

Table 4
Some global reactivity descriptors computed for the title compound.

Parameters	Values
E_{LUMO} (eV)	-6.235
E_{HOMO} (eV)	-8.822
Energy bandgap $\|E_{HOMO}- E_{LUMO}\|$	2.587
Ionization potential (I)	8.822
Electron affinity (A)	6.235
Chemical hardness	1.293
Chemical softness	0.387
Electronegativity	7.529
Chemical potential	-7.529
Electrophilicity index	21.912
Max. Charge transfer index (ΔNmax.)	5.821

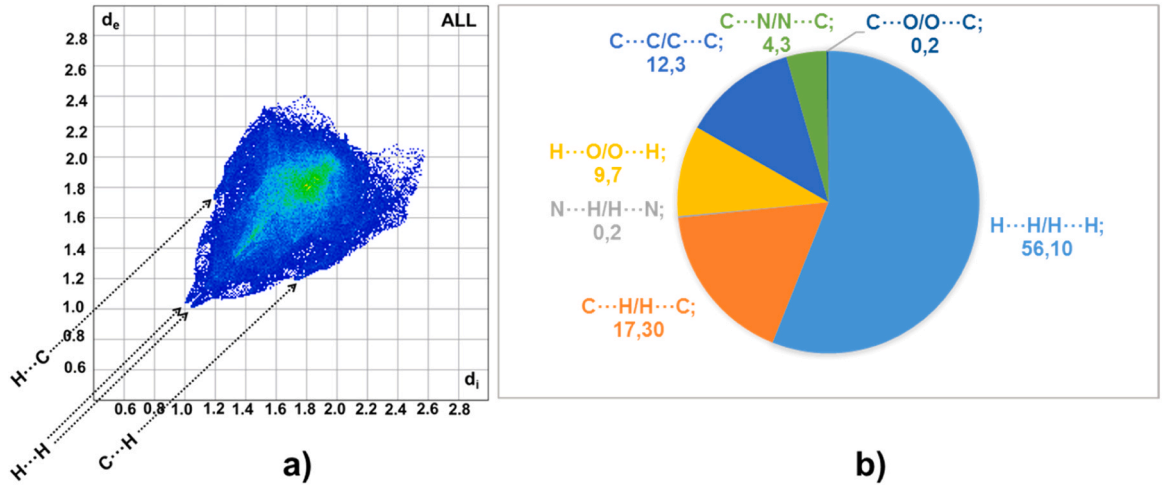


Fig. 5. a) Fingerprint plot of the compound, b) the percentage of contacts.

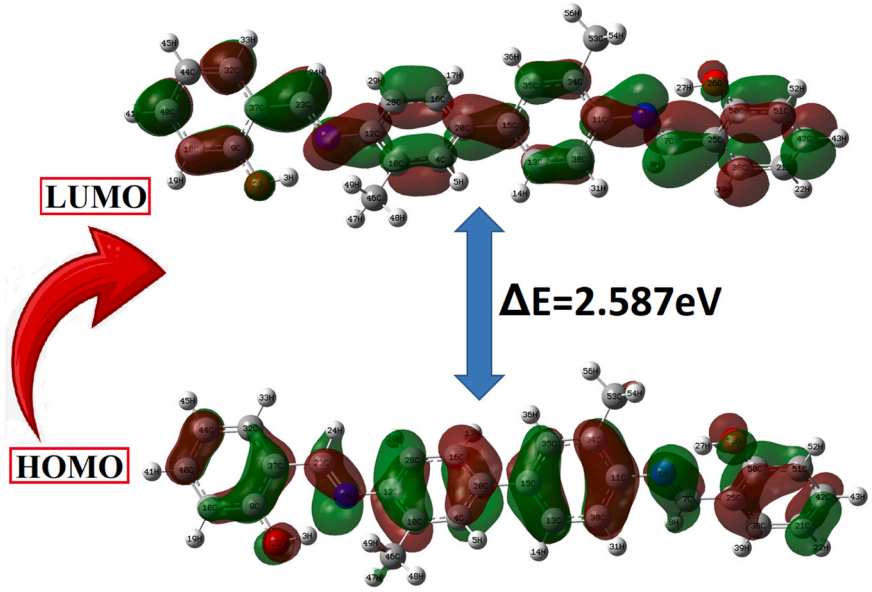


Fig. 6. LUMOs and HOMOs plots of the compound.

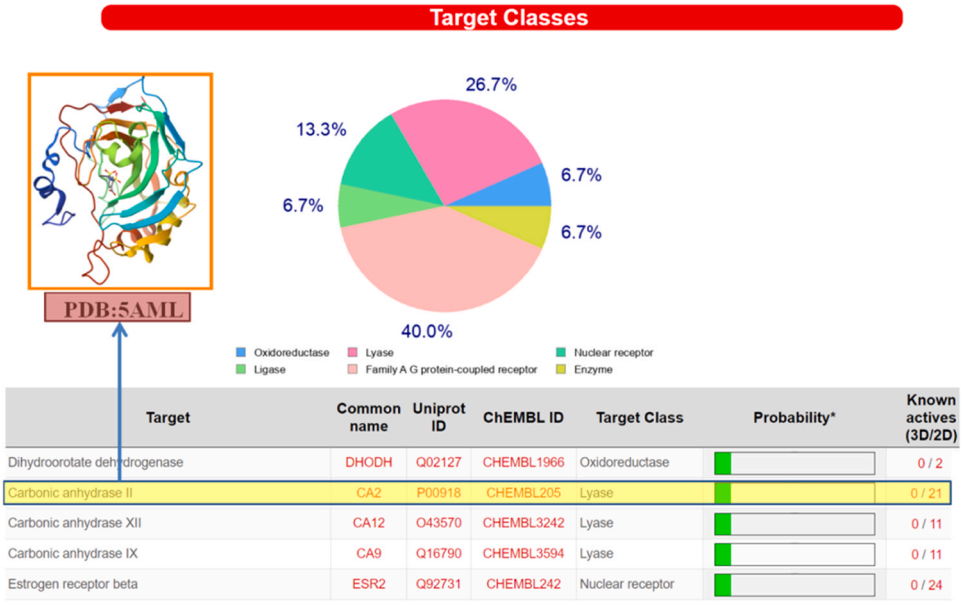


Fig. 7. SwissTarget results for our ligand.

Table 5
AutoDockVina results of the binding affinity and RMSD values of different poses in 5AML-A chain inhibitor of the title compound.

Mode	Affinity (kcal/mol)	rmsdl.b.	rmsdu.b.
1	-8.8	0.000	0.000
2	-8.6	0.734	1.458
3	-8.6	8.603	10.520
4	-8.6	8.681	10.869
5	-8.4	0.462	12.389
6	-8.3	8.674	13.457
7	-8.0	2.193	2.933
8	-7.9	9.520	12.517
9	-7.8	9.544	12.208
10	-7.8	9.652	12.043

database [23].

Six physicochemical variables were considered for a quick assessment of drug-likeness using the bioavailability radar (Fig. 9(a)). These properties were lipophilicity, size, polarity, solubility, flexibility, and saturation. When these boundaries are tested as shown in Fig. 9(a), only the saturation point and a very small part of the lipophilicity point of our molecule are excluded. For the purpose of drug development and discovery, the BOILED-Egg model provides a quick, simple, reproducible, and statistically unprecedented robust way to predict small molecule passive gastrointestinal absorption and brain access [23,56,57]. For our compound, the boiled egg model was obtained as in Fig. 9(b). According to the obtained graph, the molecule was detected as PGP+ (P-glycoprotein blue) exactly at the border of the gray and white region. Blue-colored points correspond to substances that are thought to be P-glycoprotein (PGP+) substrates and are therefore actively pumped up from the brain or the gastrointestinal lumen [23].

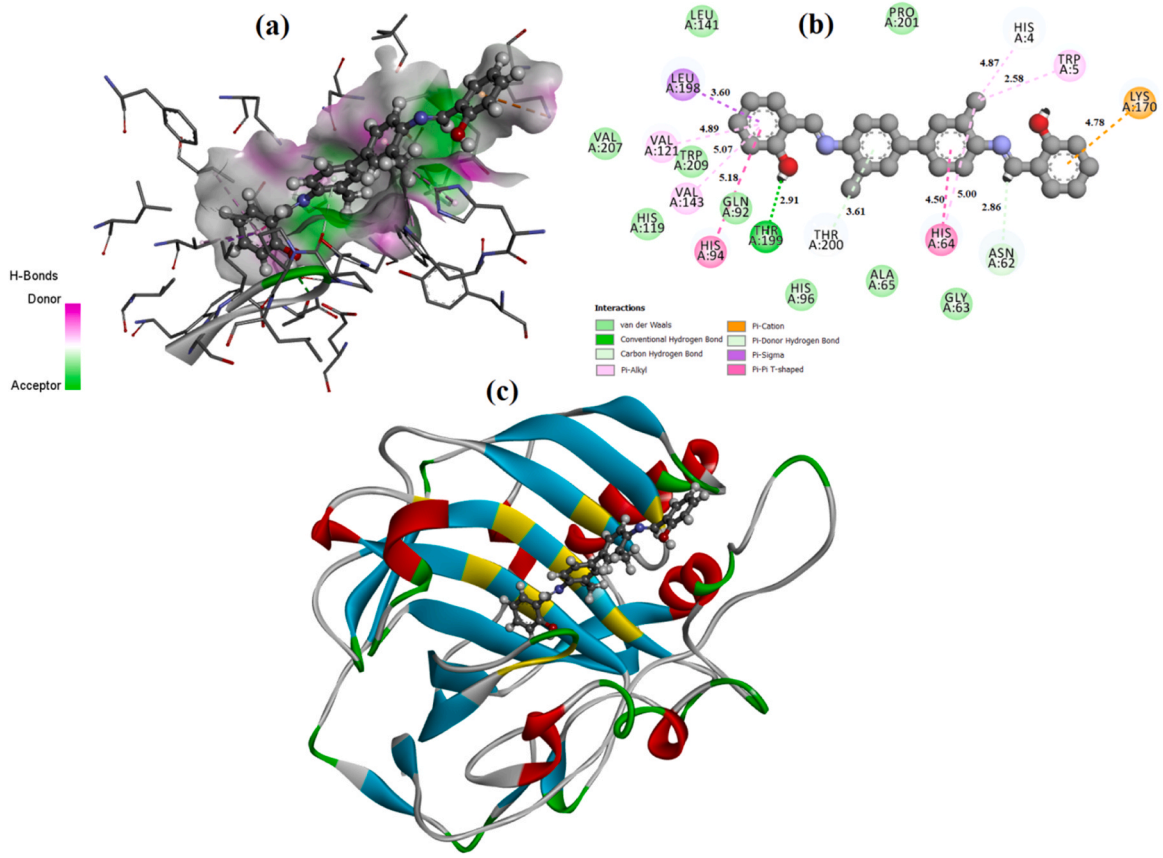


Fig. 8. The 3D (b), 2D (c) shapes of the docking and the position of the molecule within the protein (c).

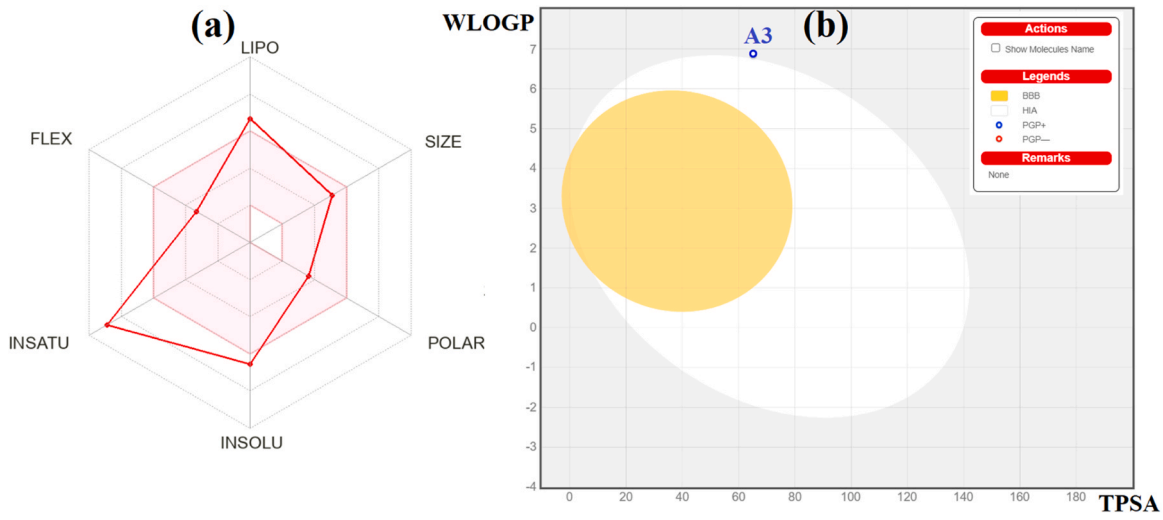


Fig. 9. The bioavailability radar (a) and the boiled-egg shape (b) of the title compound.

7. Vibrational assignments

The amount of vibrations in polyatomic molecules varies based on their chemical structure and atomic number. The literature [58,59] states that a system containing N atoms has 3 N–6 vibration modes. 3 N-6=3*56–6=162 indicates that there are 162 vibrational modes and 56 atoms in the molecule. The vibrational modes of 82 of these 162 vibrations (other vibrational modes are not included because they involve out-of-plane motion) and their theoretical assignments and corresponding experimental values were given in Table 2. Fig. 10 also displayed experimental FT-IR spectra (a) and theoretical (b). All vibrational frequencies were computed using the Gaussian 09 W package program [14], and the estimated harmonic frequencies were scaled by 0.9614 (B3LYP) for the 6–311++G(d,p) basis level [60]. Here, theoretical vibrational mode assignments for isolated molecules in the ground state and gas phase were carried out with the use of the VEDA4 program [20,21]. Based on the findings, we may conclude that experiment and theory are now in excellent agreement. The phase difference is the only cause of the variations. Generally, the OH stretching vibrations are seen between 3500 and 3300 cm^{-1}. The chemical environment has a

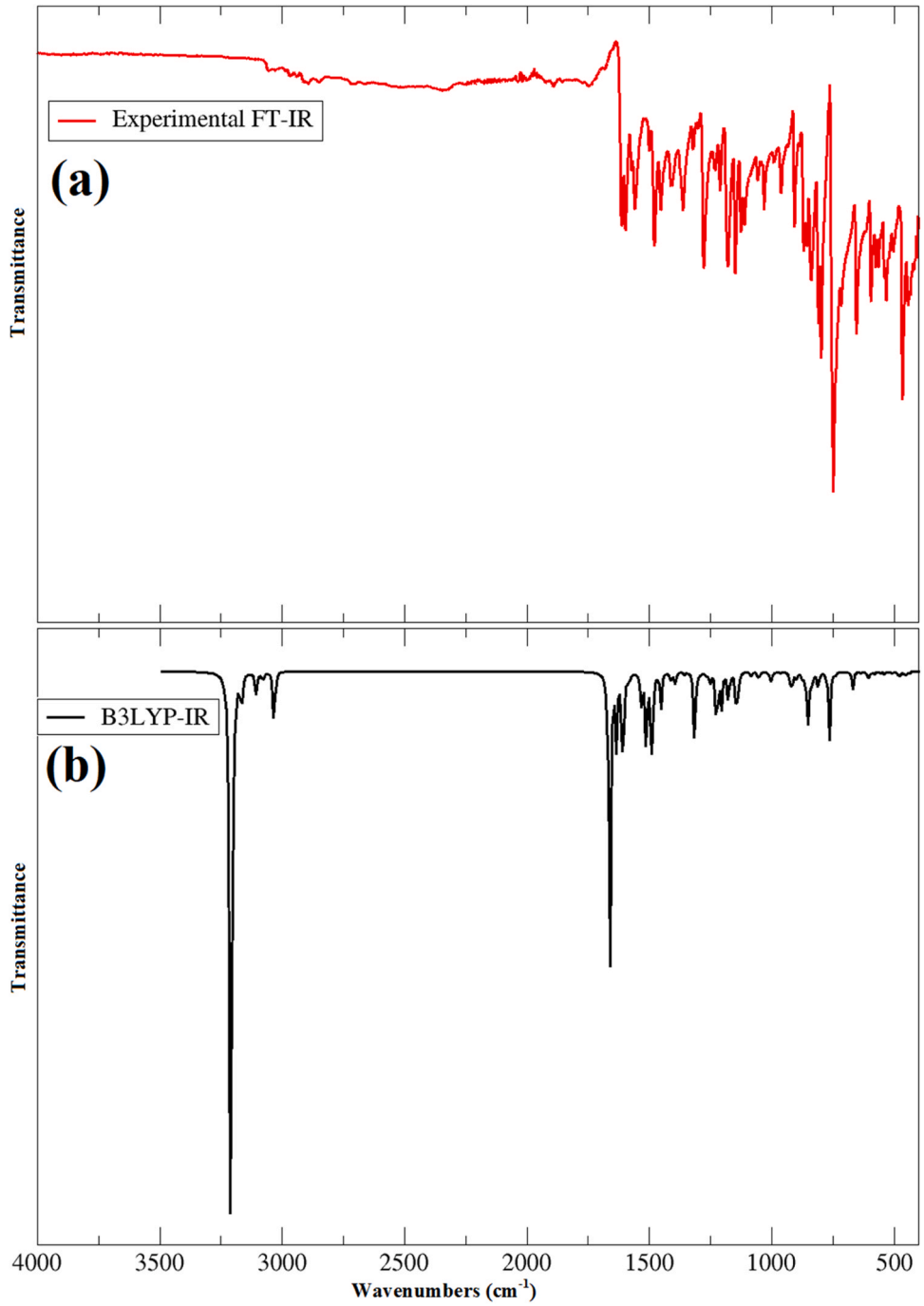


Fig. 10. The Experimental (a) and theoretical (b) spectrum of the title compound.

significant impact on this absorption, especially when OH groups are present in intramolecular or intermolecular hydrogen bonds [61,62]. In our molecule these OH bands could not be observed in experimental FT-IR, but these modes were calculated at 3090 and 3085 cm^{-1} with DFT/B3LYP/6–311++G(d,p). Table 6

In the literature, the aromatic C-H ring's stretching vibrations are often seen between 3100 and 3000 cm^{-1}. The bands in this region are not significantly affected by the type of substituent [63,64]. In our study, aromatic C-H stretching modes were computed at 3074, 3068, 3063, 3062, 3048, 3047, 3044, 3043, 3037 and 3036 cm^{-1} with DFT/B3LYP/6–311++G(d,p). These aromatic stretchings were observed at 3061 cm^{-1} in experimental FT-IR spectra. In our molecule, νCH (C23-H24 and C7-H8) modes were calculated at 2919 and 2918 cm^{-1} with DFT/B3LYP/6–311++G(d,p), also this mode were assigned at 2937 cm^{-1} in experimental FT-IR spectra. For the aliphatic C–H groups (e.g., CH3), the asymmetrical and symmetrical stretching vibrations were assigned at 3000–2905 cm^{-1} and 2870–2860 cm^{-1}, respectively [63,65]. In our system, asymmetric νCH3 modes were calculated at 2987, 2986, 2961 and 2960 cm^{-1} and symmetric νCH3 modes was calculated at 2913 cm^{-1}. These modes were observed at 2980 and 2916 cm^{-1} in experimental FT-IR spectrum, respectively.

8. Conclusions

The following is a quick description of the outcomes that were assessed during this study:

Table 6
Observed and calculated some important vibrational frequencies of A3 compound with 6–311++G(d,p).

Vib. No.	Experimental	B3LYP	Assignments
ν_1		3090	νOH(98) in the O26-H27
ν_2		3085	νOH(94) in the O2-H3
ν_3	3061	3074	νCH(100) in the ring
ν_4		3074	νCH(100) in the ring
ν_5		3068	νCH(198) in the ring
ν_6		3068	νCH(100) in the ring
ν_7		3063	νCH(95) in the ring
ν_8		3062	νCH(90) in the ring
ν_9		3048	νCH(87) in the ring
ν_{10}		3048	νCH(100) in the ring
ν_{11}		3048	νCH(98) in the ring
ν_{12}		3047	νCH(99) in the ring
ν_{13}		3044	νCH(92) in the ring
ν_{14}		3043	νCH(90) in the ring
ν_{15}		3037	νCH(90) in the ring
ν_{16}		3036	νCH(94) in the ring
ν_{17}	2980	2987	νasymCH3(95) in the $C_{46}H_{47,48,49}$
ν_{18}		2986	νasymCH3(90) in the $C_{53}H_{54,55,56}$
ν_{19}		2961	νasymCH3(92) in the $C_{46}H_{47,48,49}$
ν_{20}		2960	νasymCH3(86) in the $C_{53}H_{54,55,56}$
ν_{21}	2937	2919	νCH(92) in the C23-H24
ν_{22}		2918	νCH(95) in the C7-H8
ν_{23}	2916	2913	νsymCH3(92) in the $C_{46}H_{47,48,49}$
ν_{24}		2913	νsymCH3(81) in the $C_{53}H_{54,55,56}$
ν_{25}	1596	1599	νCC(54) in the ring+δHOC(24) in the H27-O26-C50
ν_{26}		1598	νCC(51) in the ring+δHOC(18) in the H3-O2-C9
ν_{27}		1598	νCC(50) in the ring+δHOC(11) in the H3-O2-C9
ν_{28}		1597	νC═N(46) in the N1-C7/N6═C23+δHCN(11) in the H8-C7-N1/H24-C23-N6
ν_{29}	1575	1573	νCC(37) in the ring+δHCC(11)
ν_{30}		1568	νCC(29) in the ring+δHCC(12)
ν_{31}		1547	νCC(21) in the ring+δHCC(11)
ν_{32}	1557	1546	νCC(20) in the ring+δHCC(18)
ν_{33}		1538	νCC(28) in the ring+δHCC(10)
ν_{34}		1523	νCC(19) in the ring+δHCC(10)+δHOC(11)
ν_{35}	1480	1479	δHCC(20)+δHOC(11)+τHCCC(10)
ν_{36}		1474	δHCC(10)+δHOC(10)+τHCCC(10)
ν_{37}		1469	δHCC(12)+δHOC(11)+τHCCC(10)
ν_{38}	1448	1455	τHCCC(70)
ν_{39}		1437	τHCCC(47)
ν_{40}		1435	τHCCC(67)
ν_{41}	1416	1432	νCC(40) in the ring+δHOC(12) in the H27-O26-C50
ν_{42}		1431	νCC(30) in the ring+δHOC(10) in the H27-O26-C50
ν_{43}		1426	τHCCC(80)
ν_{44}		1426	τHCCC(85)
ν_{45}		1398	δHCC(56)+δHOC(25) in the H27-O26-C50
ν_{46}		1397	δHCC(44)+δHOC(17) in the H27-O26-C50
ν_{47}		1395	δHCC(40)+δHOC(11) in the H27-O26-C50
ν_{48}	1360	1363	τHCHH(89)
ν_{49}		1362	τHCHH(92)
ν_{50}		1356	δHCC(49)+νCC(22) in the ring
ν_{51}	1321	1341	δHCC(39)+νCC(12) in the ring
ν_{52}		1340	δHCN(80)
ν_{53}		1303	δHCN(69)
ν_{54}		1302	νCC(78) in the ring
ν_{55}		1283	νCC(71) in the ring
ν_{56}	1271	1267	νCC(60) in the ring
ν_{57}		1265	νOC(60) in the O26-C50/O2-C9
ν_{58}		1265	νOC(56) in the O26-C50/O2-C9
ν_{59}		1260	δHCC(68)
ν_{60}		1246	δHCC(49)
ν_{61}	1225	1238	δHCC(71)
ν_{62}		1217	δHCC(44)
ν_{63}		1217	δHCC(62)
ν_{64}		1206	δHCC(60)
ν_{65}		1204	δHCC(71)
ν_{66}	1172	1178	δHCC(78)
ν_{67}		1174	δHCC(69)
ν_{68}		1159	δHCC(60)
ν_{69}	1148	1144	δHCC(72)
ν_{70}	1120–1052	1132	δHCC(58)
ν_{71}		1132	δHCC(82)
ν_{72}		1101	δHCC(40)
ν_{73}		1097	δHCC(56)
ν_{74}		1095	δHCC(24)

(*continued on next page*)

Table 6 (*continued*)

Vib. No.	Experimental	B3LYP	Assignments
ν_{75}		1094	δHCC(48)
ν_{76}		1043	τHCCC(70)
ν_{77}	1031	1019	τHCCC(58)
ν_{78}		1018	τHCCC(53)
ν_{79}		1011	τHCCC(70)
ν_{80}		1010	τHCCC(62)
ν_{81}	989	980	δHCC(24)+τHCCC(10)
ν_{82}	961	970	δHCC(36)+τHCCC(14)

- Crystallographic analysis was conducted.
- The newly synthesized molecule was subjected to both theoretical and experimental vibrational analysis using the 6–311++G(d,p) basis set and the B3LYP functional. Gaussian 09 W was used to calculate the harmonic wavenumbers, and VEDA 4 was used to assign the associated wavenumbers.
- The crystal structure and molecular packing most likely interactions were identified by Hirshfeld surface analysis.
- MEP analysis was used to identify the most positive and most negative locations on the whole molecule. Additionally frontier molecular orbital analysis was conducted over the optimized structure.
- The title chemical may have inhibitory effect against carbonic anhydrases II, according to the molecular docking data (PDB ID 5AML). Compared to carbonic anhydrases II, it was found to be more effective based on theoretical in silico-based docking scores.
- Drug-Likeness properties and ADME analysis of the molecule were researched in detailed.

CRediT authorship contribution statement

Dege Necmi: Writing – original draft, Methodology, Investigation, Data curation. **Albayati Mustafa R.:** Writing – original draft, Methodology, Investigation. **Şen Fatih:** Writing – original draft, Software, Conceptualization. **SERT YUSUF:** Writing – review & editing, Writing – original draft, Visualization, Validation, Supervision, Software, Resources, Project administration, Methodology, Investigation, Funding acquisition, Formal analysis, Data curation, Conceptualization.

Declaration of Competing Interest

This manuscript has not been submitted to, nor is under review at, another journal or other publishing venue.

Data Availability

The data that has been used is confidential.

References

[1] A. Kajal, S. Bala, S. Kamboj, N. Sharma, V. Saini, Schiff bases: a versatile pharmacophore, J. Catal. 2013 (2013).
[2] Z. Cimerman, S. Miljanić, N. Galić, Schiff bases derived from aminopyridines as spectrofluorimetric analytical reagents, Croat. Chem. Acta 73 (2000) 81–95.
[3] A. Jarrahpour, D. Khalili, Synthesis of some new bis-Schiff bases of isatin and 5-fluoroisatin in a water suspension medium, Molecules 11 (2006) 59–63.
[4] A.A.A.-Aa S.A.Karim, Synthesis and characterization of new (Bis) Schiff base derivatives based on adamantane and evaluation antioxidant activity, Eurasia Chem. Commun. 5 (2023).
[5] I. Arshad, A. Saeed, P.A. Channar, S.A. Shehzadi, M.N. Ahmed, M. Siddiq, Bis-Schiff bases of 2, 2′-dibromobenzidine as efficient corrosion inhibitors for mild steel in acidic medium, RSC Adv. 10 (2020) 4499–4511.
[6] M. Arshad, S. Arshad, M.K. Majeed, J. Frueh, C. Chang, I. Bilal, S.I. Niaz, M. S. Khan, M.A. Tariq, M. Yasir Mehboob, Transition metal-decorated Mg12O12 nanoclusters as biosensors and efficient drug carriers for the metformin anticancer drug, ACS Omega 8 (2023) 11318–11325.
[7] D. Iacopetta, J. Ceramella, A. Catalano, C. Saturnino, M.G. Bonomo, C. Franchini, M.S. Sinicropi, Schiff bases: Interesting scaffolds with promising antitumoral properties, Appl. Sci. 11 (2021) 1877.
[8] S. Shokrollahi, A. Amiri, F. Fadaei-Tirani, K. Schenk-Joß, Promising anti-cancer potency of 4, 5, 6, 7-tetrahydrobenzo [d] thiazole-based Schiff-bases, J. Mol. Liq. 300 (2020) 112262.
[9] N.M. Morsy, A.S. Hassan, T.S. Hafez, M.R. Mahran, I.A. Sadawe, A.M. Gbaj, Synthesis, antitumor activity, enzyme assay, DNA binding and molecular docking of Bis-Schiff bases of pyrazoles, J. Iran. Chem. Soc. 18 (2021) 47–59.
[10] S. Kumar, S.M. Lim, K. Ramasamy, M. Vasudevan, S.A.A. Shah, M. Selvaraj, B. Narasimhan, Synthesis, molecular docking and biological evaluation of bis-pyrimidine Schiff base derivatives, Chemistry Central, Chem. Central J. 11 (2017) 1–16.
[11] H.A. Mohammed, Y. Sert, M.R. Albayati, N. Dege, F. Şen, Structure Elucidation, Hirshfeld Surface Analysis, Molecular Docking and Computational Studies of a Jahn-Teller Distorted Octahedral Cobalt (II) Complex with Saccharin Ligand, Polycycl. Aromat. Compd. 43 (2023) 4396–4406.
[12] M.R. Albayati, S. Kansız, H. Lgaz, S. Kaya, N. Dege, I.H. Ali, R. Salghi, I.-M. Chung, Synthesis, experimental and theoretical characterization of (*E*)-2-((2, 3-dimethylphenyl) amino)-N'-(furan-2-ylmethylene) benzohydrazide, J. Mol. Struct. 1219 (2020) 128518.
[13] M.R. Albayati, S. Kansız, N. Dege, S. Kaya, R. Marzouki, H. Lgaz, R. Salghi, I.H. Ali, M.M. Alghamdi, I.-M. Chung, Synthesis, crystal structure, Hirshfeld surface analysis and DFT calculations of 2-[(2, 3-dimethylphenyl) amino]-N'-[(*E*)-thiophen-2-ylmethylidene] benzohydrazide, J. Mol. Struct. 1205 (2020) 127654.
[14] M.J. Frisch, G. Trucks, H. Schlegel, G. Scuseria, M. Robb, J. Cheeseman, G. Scalmani, V. Barone, B. Mennucci, G. Petersson, Gaussian 09, Revision D. 01, Gaussian, Inc.: Wallingford, CT (2009).
[15] T. Van Mourik, M. Bühl, M.-P. Gaigeot, Density functional theory across chemistry, physics and biology, R. Soc. Publ. (2014) 20120488.
[16] T. van Mourik, M. Bühl, M.-P. Gaigeot, Density functional theory across chemistry, Physics and Biology, R. Soc. (2014).
[17] A.D. Becke, A new mixing of Hartree–Fock and local density-functional theories, J. Chem. Phys. 98 (1993) 1372–1377.
[18] A.D. Becke, Density-functional exchange-energy approximation with correct asymptotic behavior, Phys. Rev. A 38 (1988) 3098.
[19] R. Dennington, T. Keith, J. Millam, GaussView, version 5, Semichem Inc.: Shawnee Mission, KS (2009).
[20] M.H. Jamroz, Vibrational energy distribution analysis VEDA 4, Wars. Pol. (2004).
[21] M.H. Jamróz, Vibrational energy distribution analysis (VEDA): scopes and limitations, Spectrochim. Acta Part A: Mol. Biomol. Spectrosc. 114 (2013) 220–230.
[22] M. Turner, J. McKinnon, S. Wolff, D. Grimwood, P. Spackman, D. Jayatilaka, M. Spackman, CrystalExplorer17; University of Western Australia: Crawley, WA, Australia, 2017, There is no corresponding record for this reference.[Google Scholar].
[23] A. Daina, O. Michielin, V. Zoete, SwissADME: a free web tool to evaluate pharmacokinetics, drug-likeness and medicinal chemistry friendliness of small molecules, Sci. Rep. 7 (2017) 1–13.
[24] O. Trott, A.J. Olson, AutoDock Vina: improving the speed and accuracy of docking with a new scoring function, efficient optimization, and multithreading, J. Comput. Chem. 31 (2010) 455–461.
[25] G. Sheldrick, SHELXL-97, Program for crystal structure refinement; University of Göttingen: Göttingen, Germany, 1997, SHELXL-97, Program for crystal structure refinement; University of Göttingen: Göttingen, Germany, 1997, (1997).
[26] G.M. Sheldrick, Crystal structure refinement with SHELXL, Acta Crystallogr. Sect. C: Struct. Chem. 71 (2015) 3–8.
[27] L.J. Farrugia, WinGX and ORTEP for Windows: an update, J. Appl. Crystallogr. 45 (2012) 849–854.
[28] (a) M. Nardelli, Comput. Chem. 7 (1983) 95–98;
(b) M. Nardelli, J. Appl. Cryst. 28 (1995) 659.
[29] M. Nardelli, PARST95–an update to PARST: a system of Fortran routines for calculating molecular structure parameters from the results of crystal structure analyses, J. Appl. Crystallogr. 28 (1995), 659-659.
[30] Ş. ATALAY, X-Ray and Theoretical Studies of 4-((4-(tert-butyl) benzylidene) amino)-1, 5-dimethyl-2-phenyl-1, 2-dihydro-3H-pyrazol-3-one, Süleyman Demirel Üniversitesi Fen Edebiyat Fakültesi Fen Dergisi, 13 (2018) 108-120.
[31] Ö. Kalfa, F. Tekin, B. Koşar, C.C. Ersanlı, 2-HİDROKSİ-6-[(4-HİDROKSİFENİLAMİNO) METİLEN] SİKLOHEKZA-2, 4-DİYENON'UN KUANTUM KİMYASAL HESAPLAMALARI ÜZERİNE BİR ÇALIŞMA, J. Sci. Technol. DumlupıNar. Univ. (2016) 127–138.
[32] Ş. Pınar, S. KANSIZ, D. Necmi, synthesis, molecular structure, hirshfeld surface analysis, spectroscopic and computational studies (DFT) of 6, 6′-((1E, 1′E)-(1, 2-phenylenebis (azanylylidene)) bis (methanylylidene)) bis (2-(tert-butyl)-4-methylphenol), J. Turk. Chem. Soc. Sect. A: Chem. 6 (2019) 189–200.

[33] M.A. Spackman, D. Jayatilaka, Hirshfeld surface analysis, CrystEngComm 11 (2009) 19–32.
[34] Y.-H. Luo, C.-G. Zhang, B. Xu, B.-W. Sun, A cocrystal strategy for the precipitation of liquid 2, 3-dimethyl pyrazine with hydroxyl substituted benzoic acid and a Hirshfeld surfaces analysis of them, CrystEngComm 14 (2012) 6860–6868.
[35] P. Singh, R. Kant, S.D. Sharma, Crystal Structure and Hirshfeld Surface Investigation of 3, 4-bis (prop-2-yn-1-yloxy) benzaldehyde.
[36] S. Shit, C. Marschner, S. Mitra, Synthesis, Crystal structure, and Hirshfeld Surface Analysis of a New Mixed Ligand Copper (II) Complex, Acta Chim. Slov. 63 (2016).
[37] P.R. Spackman, M.J. Turner, J.J. McKinnon, S.K. Wolff, D.J. Grimwood, D. Jayatilaka, M.A. Spackman, CrystalExplorer: A program for Hirshfeld surface analysis, visualization and quantitative analysis of molecular crystals, J. Appl. Crystallogr. 54 (2021) 1006–1011.
[38] K. Fukui, Role of frontier orbitals in chemical reactions, science 218 (1982) 747–754.
[39] R.G. Parr, R.G. Pearson, Absolute hardness: companion parameter to absolute electronegativity, J. Am. Chem. Soc. 105 (1983) 7512–7516.
[40] C.-G. Zhan, J.A. Nichols, D.A. Dixon, Ionization potential, electron affinity, electronegativity, hardness, and electron excitation energy: molecular properties from density functional theory orbital energies, J. Phys. Chem. A 107 (2003) 4184–4195.
[41] P. Geerlings, F. De Proft, W. Langenaeker, Conceptual density functional theory, Chem. Rev. 103 (2003) 1793–1874.
[42] R.G. Pearson, Absolute electronegativity and hardness: applications to organic chemistry, J. Org. Chem. 54 (1989) 1423–1430.
[43] R.G. Parr, Lv Szentpály, S. Liu, Electrophilicity index, J. Am. Chem. Soc. 121 (1999) 1922–1924.
[44] J.C. Costa, R.J. Taveira, C.F. Lima, A. Mendes, L.M. Santos, Optical band gaps of organic semiconductor materials, Opt. Mater. 58 (2016) 51–60.
[45] B.J. McConkey, V. Sobolev, M. Edelman, The performance of current methods in ligand–protein docking, Curr. Sci. (2002) 845–856.
[46] N. Dege, H. Gökce, O.E. Doğan, G. Alpaslan, T. Ağar, S. Muthu, Y. Sert, Quantum computational, spectroscopic investigations on N-(2-((2-chloro-4, 5-dicyano-phenyl) amino) ethyl)-4-methylbenzenesulfonamide by DFT/TD-DFT with different solvents, molecular docking and drug-likeness researches, Colloids Surf. A: Physicochem. Eng. Asp. 638 (2022) 128311.
[47] M. Gümüş, Ş.N. Babacan, Y. Demir, Y. Sert, İ. Koca, İ. Gülçin, Discovery of sulfadrug–pyrrole conjugates as carbonic anhydrase and acetylcholinesterase inhibitors, Arch. Der Pharm. 355 (2022) 2100242.
[48] J. Ivanova, J. Leitans, M. Tanc, A. Kazaks, R. Zalubovskis, C.T. Supuran, K. Tars, X-ray crystallography-promoted drug design of carbonic anhydrase inhibitors, Chem. Commun. 51 (2015) 7108–7111.
[49] I. Mahmudov, Y. Demir, Y. Sert, Y. Abdullayev, A. Sujayev, S.H. Alwasel, I. Gulcin, Synthesis and inhibition profiles of N-benzyl-and N-allyl aniline derivatives against carbonic anhydrase and acetylcholinesterase–A molecular docking study, Arab. J. Chem. 15 (2022) 103645.
[50] U. Atmaca, R. Saglamtas, Y. Sert, M. Çelik, İ. Gülçin, Metal-free synthesis via intramolecular cyclization, enzyme inhibition properties and molecular docking of novel isoindolinones, ChemistrySelect 8 (2023) e202204578.
[51] ⟨http://www.swisstargetprediction.ch/⟩.
[52] ⟨https://www.rcsb.org/⟩.
[53] ⟨http://www.3dsbiovia.com/⟩.
[54] C.A. Lipinski, F. Lombardo, B.W. Dominy, P.J. Feeney, Experimental and computational approaches to estimate solubility and permeability in drug discovery and development settings, Adv. Drug Deliv. Rev. 23 (1997) 3–25.
[55] C.A. Lipinski, Drug-like properties and the causes of poor solubility and poor permeability, J. Pharmacol. Toxicol. Methods 44 (2000) 235–249.
[56] C.M. Hansen, The three dimensional solubility parameter, Dan. Tech.: Cph. 14 (1967).
[57] C.M. Hansen, Hansen solubility parameters: a user's handbook, CRC press2007.
[58] A. Katritzky, The infrared spectra of heteroaromatic compounds, Q. Rev., Chem. Soc. 13 (1959) 353–373.
[59] A.E. Segneanu, I. Gozescu, A. Dabici, P. Sfirloaga, Z. Szabadai, Organic compounds FT-IR spectroscopy, InTech Romania2012.
[60] D. Young, Computational chemistry: a practical guide for applying techniques to real world problems, John Wiley & Sons, 2004.
[61] M. Ladetto, M. Márquez, D. Romani, S. Brandán, Structural and vibrational studies on isomers of antiviral ribavirin drug in gas and aqueous environmental by using the SQM approach, J. Adv. Chem. 16 (2019) 6325–6353.
[62] D. Douche, Y. Sert, S.A. Brandán, A.A. Kawther, B. Bilmez, N. Dege, A. El Louzi, K. Bougrin, K. Karrouchi, B. Himmi, 5-((1H-imidazol-1-yl) methyl) quinolin-8-ol as potential antiviral SARS-CoV-2 candidate: synthesis, crystal structure, Hirshfeld surface analysis, DFT and molecular docking studies, J. Mol. Struct. 1232 (2021) 130005.
[63] R. Silverstein, F. Webster, Spectroscopic Identification of Organic Compounds, John Wiley & Sons, New York, 1997.
[64] Y. Sert, O.E. Doğan, H. Gökce, T. Ağar, F. Ucun, N. Dege, Synthesis, crystal structure, Hirshfeld surface analysis, spectral characterization, and quantum computational evaluation of (*E*)-2-(((4-bromophenyl) imino) methyl)-6-methylphenol, J. Phys. Chem. Solids 144 (2020) 109478.
[65] G. Varsányi, Assignments for vibrational spectra of seven hundred benzene derivatives, Halsted Press1974.